Saturation of surface roughening instabilities by plastic deformation

Michael Andersen,[1,a)] Nasr Ghoniem,[1] and Akiyuki Takahashi[2]
[1]*Department of Mechanical and Aerospace Engineering, University of California, Los Angeles, California 90095-1597, USA*
[2]*Department of Mechanical Engineering, Faculty of Science and Technology, Tokyo University of Science, Chiba 278–8510, Japan*

(Received 4 December 2007; accepted 22 January 2008; published online 26 February 2008)

Surface roughening instabilities driven by a competition between elastic and surface energy contributions are shown to be saturated by plastic energy dissipation. It is shown that these morphological instabilities do not experience unbounded growth as predicted by consideration of elastic energy alone and that their growth is limited by dislocation emission from higher curvature grooves. © *2008 American Institute of Physics*. [DOI: 10.1063/1.2842412]

Roughening phenomena of stressed solid surfaces are important in applications such as chemical etching,[1] heteroepitaxial thin film growth,[2] solidification,[3] stress corrosion cracking,[4] etc. A flat surface is unstable to morphological perturbations on the surface.[5] Under these conditions, it has been recognized that the driving force for the instability is the reduction in the elastic energy of the solid when its surface becomes corrugated, in agreement with the Griffith fracture criterion of brittle solids.[5] Thus, flat surfaces tend to develop cusps and valleys when a threshold level of stress is applied. Based on the Griffith concept of fracture,[5] several models have been proposed to explain the development of surface roughness in essentially flat surfaces. Asaro and Tiller[6] and Grinfeld[7] have advanced the basic concepts behind stress-driven surface instabilities, in what is known as the Asaro–Tiller–Grinfeld (ATG) instability. Gao *et al.*[8] followed similar evaluations utilizing perturbation theory to investigate the initial growth stages of surface grooves. Recent numerical assessments include application of phase field theory to the problem of morphological instabilities during melting and solidification.[9] In addition, Yang and Srolovitz[10] developed a numerical method for the later stages of surface crack growth instabilities.

In ductile materials, experimental observations indicate that surface instabilities do not experience unbounded growth, as predicted by either perturbation theory,[8] or numerical treatments.[10] Moreover, numerical methods designed to capture the later stages of grooving breakdown when the groove tip curvature becomes sharp.[9,11] We show here that stress-driven grooving instabilities will not develop into cusps and that the growth rate of these instabilities is saturated as a result of energy dissipation in the nucleation and motion of subsurface dislocations. We present here a surface roughening model that accounts for plastic energy dissipation. First, we verify the numerics of the model by comparing to the predictions of perturbation theory[8] and to the numerical solutions of Yang and Srolovitz.[10,12] Then, we account for plastic energy dissipation and show the effects of dislocation emission from stressed surfaces on the growth of roughening instabilities. Finally, we present numerical results showing that the growth rate of surface roughening perturbations becomes almost constant rather than exponential as a result of dislocation emission.

Consider the upper surface of a semi-infinite uniaxially stressed solid to be periodic, $y=h(x)$, with amplitude and wavelength A and λ, respectively. The surface is free of tractions. The solid is then subjected to a biaxial bulk stress σ^{∞}. The boundary integral equation for the displacement field $u(\xi)$ at a point ξ in the solid is given by Ref. 10 as

$$u_i(\xi) = 2\left[u_i^{\infty}(\xi) - \int_s \bar{T}_{ij}(x,\xi) u_j(\xi) dS(x) \right], \tag{1}$$

where u^{∞} is the displacement associated with the bulk stress and $\bar{T}_{ij}$ is the elastic Green's function that satisfies the periodic boundary conditions.[12] The surface is modeled with a cubic spline function to keep C-2 continuity, which will be important for calculating curvature along the surface. The stress field can be calculated using Hooke's law, which provides the elastic strain energy density as $\omega_e=(1/2E)\sigma_{tt}^2$, where σ_{tt} is the tangential stress along the surface.

The chemical potential μ is given as $\mu=\mu^*+\gamma\Omega\kappa+\Omega\omega_e$, where μ^* is the chemical potential of a flat surface associated with the bulk stress, γ is the surface free energy, κ is the surface curvature, and Ω is the atomic volume. The Nernst–Einstein relation $J=-(D_s/kT)(\partial\mu/\partial s)$ can then be utilized to define material transport along the surface, where the diffusion flux J is related to the gradient of the chemical potential along the surface. Here, the atomic surface diffusivity is D_s, the Boltzmann's constant is k, and the temperature is T. The normal velocity of the surface is determined from the mass conservation equation[13] and the divergence of the diffusion flux as $V_n=-(D_s\Omega\nu_s/kT)(\partial^2\mu/\partial s^2)$, where ν_s is the number of atoms per unit area on the plane normal to the flux direction. The vertical component of the normal velocity[10] can be used to determine the surface profile $h(x,t)$ as

$$\frac{\partial h}{\partial t} = D\frac{\partial}{\partial x}\left[(1+h_{,x}^2)^{-1/2}\frac{\partial}{\partial x}(\gamma\kappa+\omega_e) \right], \tag{2}$$

where $D=D_s\Omega^2\nu_s/kT$ and $h_{,x}=\partial h/\partial x$. Surface evolution poses particular numerical difficulties because of high-order derivatives, so three-point filtering technique along with fitting cubic spline functions to the surface is used to describe surface evolution.

We first consider the results of linear perturbation theory, given an initial surface profile, $h_0=A\cos(2\pi x/\lambda)$.[10] When σ^{∞} is applied, the maximum and minimum tangential stress

a)Electronic mail: m.andersen@ucla.edu.

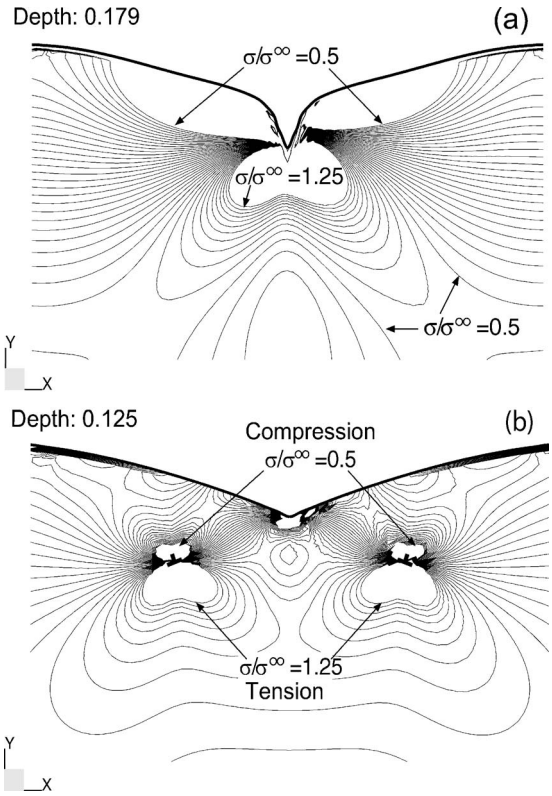

FIG. 1. The tangential stress field around the groove at $t/\tau=2.7\times10^{-5}$ is shown for a groove (a) with and (b) without dislocation emission. The initial surface as in all figures is a sine wave with $A_0/\lambda=0.05$ and $\Sigma=3$. The stress is from 0.5 to 1.25 normalized to the bulk stress.

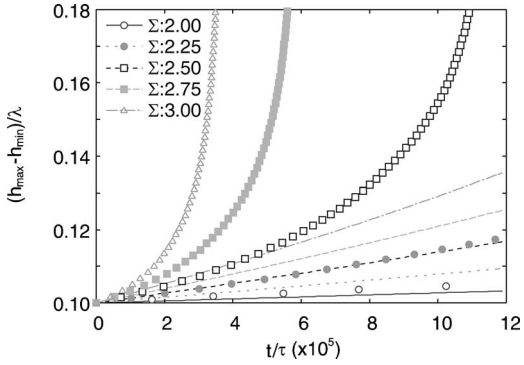

FIG. 2. The time dependence of the surface amplitude $(h_{max}-h_{min})/\lambda$ is shown for several stress values. The results for the numerical model are displayed as symbols, while the perturbation analysis is shown by lines.

is found in the valley and peak, respectively. The lowest order tangential stress at the valley and peak is found to be $\sigma_{tt}=\sigma^{\infty}(1\pm4\pi A/\lambda)$. The perturbation analysis also shows the amplitude to grow as $A(t)=A(0)e^{\alpha t}$, where the growth rate, $\alpha=D(2H\sigma^2k^3-\gamma k^4)$ and k is the wave number of the perturbation with $H=(1-\nu)/E$ for plane strain. We can then find that the surface amplitude will grow when $\sigma^{\infty}\geqslant\sqrt{\pi\gamma E/\lambda}$ or in nondimensional form $\Sigma=\sigma^{\infty}(\lambda/\gamma E)^{1/2}\geqslant\sqrt{\pi/(1-\nu^2)}$. If we take $\nu=1/3$, then perturbation theory shows that the amplitude will grow when $\Sigma_c\geqslant1.88$.[8]

To validate the present numerical solution, we compare the solution to that of Ref. 8 for the initial growth phase and Ref. 10 for the later stages. At this point, the chemical potential has only elastic energy released by grooving at the expense of the surface energy that need to be supplied when deeper grooves form. We begin with a sinusoidal surface with $A/\lambda=0.05$. Equation (1) is used to solve for the displacements. A free surface problem is setup where traction boundary conditions are used to cancel out the tractions generated from the external normal stress. The calculated displacements are then transformed into stresses along the surface through Hooke's law and ultimately into elastic strain energy. In turn, this is used to calculate the chemical potential and through Eq. (2) the movement of the surface is found. The surface is evolved with a Galerkin finite element method utilizing a backward Euler (BE) implicit time integration. The BE method is controlled by setting the growth per time step. The time is scaled as $\tau=\lambda^4/(D\gamma)$.

Figure 1(a) shows the effect on the surface at time, $t/\tau=2.7\times10^{-5}$, with σ^{∞} higher than the instability level at $\Sigma=3.0$. The groove begins to cusp quickly and forms two bumps next to the groove as has been seen in previous work.[10,12] The bumps are regions where the material diffusing out of the groove accumulates and are noted as a common feature of surface diffusion.[13] As material moves away from the area with the highest strain energy, the groove deepens steadily until the cusp is formed. Once the cusp is formed, the stress concentration increases and the groove deepens exponentially.

When we compare the growth to linear perturbation theory,[8] we find strong agreement only during the initial stages. The maximum stress is at the groove opening and the stress falls off to near zero at the adjacent peaks while most of the material is at the applied bulk stress. The perturbation results are only useful for small values of A/λ (<0.1) (Ref. 8) because the theory predicts the stress at the peaks to become negative.

In Fig. 2, the dependence of the surface profile amplitude on time is shown for the numerical model (dotted points) and linear perturbation theory (solid lines).[14] The present numerical model agrees well with perturbation theory[8] at early times, as expected, and with the numerical solutions of Ref. 10 The perturbation theory underestimates the growth rate for high stress and later time steps. It should be noted that the surface is stable for stresses below $\Sigma\leqslant\Sigma_c=1.88$, but surface perturbations decay for lower stress values. When $\Sigma=2.0$, the growth is linear and comparatively very slow, but it is indeed growing at that point. About midway through the simulation ($t/\tau\approx2.0\times10^{-5}$), the surface no longer looks sinusoidal as the cusp forms.

Next, we consider the chemical potential along the surface when the energy dissipated in plastic work is included. Here, the chemical potential is written as $\mu=\mu^*+\gamma\Omega\kappa+\Omega(\omega_e+\omega_p)$, where ω_p is the plastic strain energy density. The plastic strain energy density is calculated as the work done due to dislocation motion near surface regions of high stress concentrations. Thus, the plastic strain energy density is summed over all dislocations N_D as $\omega_p=\Sigma_i^{N_D}\sigma^{\infty}\varepsilon_i^p$, where ε_i^p is the plastic strain produced by the ith dislocation. The plastic strain is calculated by $\varepsilon_i^p=bl_i/A$, where l_i is the length swept by ith dislocation and A is the area of the plastic zone. Once the resolved shear stress on a plane oriented at 70.5° from the crack plane (maximum shear) reaches the critical resolved shear stress (CRSS), nucleated dislocations move away from the crack tip. Dislocation nucleation is possible only in ductile materials, and we adopt here the nucleation

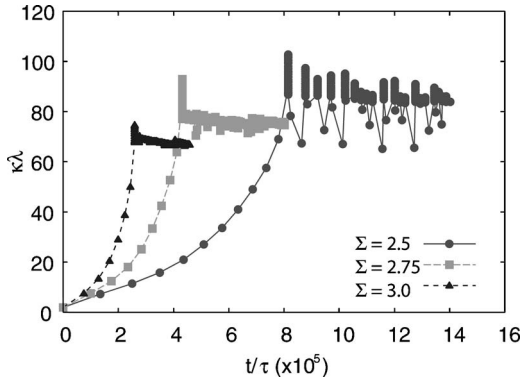

FIG. 3. The curvature normalized with the wavelength at the cusp is shown with plasticity effects for three stress values. As dislocations are emitted the curvature is decreased immediately with the dislocation emission.

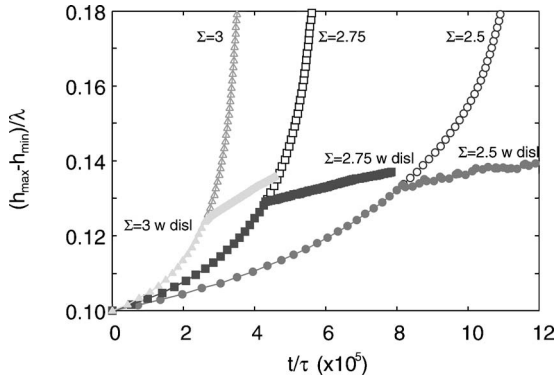

FIG. 4. The time dependence of the amplitude of the surface is shown with plasticity effects (solid symbols) and with the elastic energy contribution alone (hollow symbols). Dislocations are emitted from the tip of the groove, which change the exponential growth into a linear region.

criterion of Rice and Beltz.[15] Thus, dislocations are assumed to be nucleated when $\gamma_{us} > \gamma$, where γ_{us} is the unstable stacking fault energy.

The emitted dislocations move in the material based on dislocation dynamics (DD).[16] In the DD method, the forces on the dislocations f_i can be calculated by the Peach–Koehler formula given as $f_i = \epsilon_{ijk}\sigma_{jl}bt_k$, where ϵ_{ijk} is the permutation tensor, b is the Burgers vector, and t_k is the unit tangent vector of the dislocation. The stress σ_{ij} is the sum of the external stress, stresses generated by other dislocations and the image stress from the free surface which is the solution to Eq. (1). The stress of an infinitely straight edge dislocation is given in analytical form. The velocity of the dislocation is given by $v = v_0(\tau/\tau_0)^m$, where τ is the resolved shear stress on the slip plane of the dislocation, and v_0, τ_0, and m are the temperature dependent material constants, respectively. Since the wavelength is large compared to the Burgers vector, superdislocations are used with an effective Burgers vector of $100b$.

Figure 1(b) shows the tangential stress field contours around the groove after dislocations are emitted. These specific calculations are performed for tungsten, which has a yield stress of 550 MPa, Young's modulus of 411 GPa, and $\nu = 0.28$. Comparing Figs. 1(a) and 1(b) reveals that the surface profile and stress field distribution are significantly changed as a result of dislocation emission from the crack tip. The surface profiles are calculated at a normalized time of $t/\tau = 2.7 \times 10^{-5}$. It is seen that while the stress is all tensile and reaches values as high as 1.25 σ/σ^{∞} near the crack tip in the elastic case [Fig. 1(a)], emitted dislocations actually shield the tip from tensile stresses, as can be ascertained from Fig. 1(b). The region between emitted dislocations and the crack tip is on the compressive side of the dislocations and would, hence, tend to close the crack tip and oppose its sharpening. The surface profile is also dramatically altered from cusplike to a shallow groove.

The groove stays at relatively the same depth once dislocations are emitted while the groove without dislocation emission deepens and turns into a cusp. Emitted dislocations result in decreasing the tip curvature immediately after forming, as shown in Fig. 3. The decreased curvature relaxes the stress, but as the dislocation moves from the tip, the stress builds and the process is repeated.

The change in the growth rate of surface perturbations as a result of plasticity is illustrated in Fig. 4 where the surface amplitude is shown as a function of normalized time with and without dislocation emission. The surface no longer grows exponentially once dislocations are emitted. The growth becomes nearly linear, and the growth rate approaches a constant value after the emission of dislocations and continues so as long as dislocations are emitted.

We were able to reproduce similar results that have been witnessed in the elastic regime and with the inclusion of plasticity, we show that the classical ATG instability is saturated as a result of dislocation emission in ductile materials. The key factor in limiting surface crack growth instabilities is the ease by which dislocations are nucleated, and not their mobility. Nucleated dislocations in the vicinity of the crack tip keep the curvature from unbounded growth as a result of two mechanisms: (1) with each emitted dislocation, the crack geometry is changed by reducing the curvature and (2) emitted dislocations that linger around the crack tip induce a compressive stress (pressure) that tends to close it up. These mechanisms keep the overall growth bounded. As the dislocations move away, the stress builds until more dislocations are emitted repeating the saturation cycle.

The authors wish to acknowledge the support of The Naval Research Laboratory (NRL) (Grant No. N00173-06-1-G905) for this research.

[1] K.-S. K. J. Hurtado and H. Tan, Phys. Rev. Lett. **83**, 3872 (1999).
[2] K. Kassner and C. Misbah, Phys. Rev. E **66**, 026102 (2002).
[3] I. C. K. K. C. M. H. Muller-Krumbhaar, Phys. Rev. E **58**, 6027 (1998).
[4] D. Koehn, J. Arnold, B. Jauntreit, and A. Malthe-Sørenssen, American Journal of Science **303**, 956 (2003).
[5] A. Griffith, Philos. Trans. R. Soc. London, Ser. A **221**, 163 (1921).
[6] R. J. Asaro and A. W. Tiller, Metall. Trans. **3**, 1789 (1972).
[7] M. Grinfeld, Sov. Phys. Dokl. **31**, 831 (1986).
[8] H. Gao, Int. J. Solids Struct. **28**, 703 (1991).
[9] K. K. C. M. J. M. J. Kappey and P. Kohlert, Phys. Rev. E **63**, 036117 (2001).
[10] W. Yang and D. Srolovitz, Phys. Rev. Lett. **71**, 1593 (1993).
[11] J. Muller and M. Grant, Phys. Rev. Lett. **82**, 1736 (1999).
[12] W. Yang and D. J. Srolovitz, J. Mech. Phys. Solids **42**, 1551 (1994).
[13] W. Mullins, J. Appl. Phys. **28**, 333 (1957).
[14] D. Srolovitz, Acta Metall. **37**, 621 (1989).
[15] J. Rice and G. Beltz, J. Mech. Phys. Solids **42**, 333 (1994).
[16] L. S. N. M. Ghoniem and S. H. Tong, Phys. Rev. B **61**, 913 (2000).